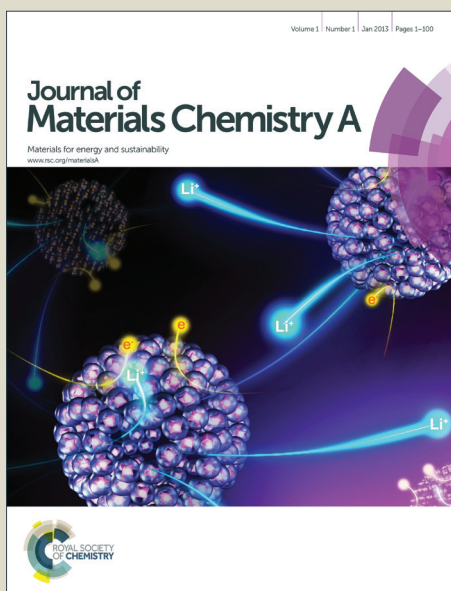


Journal of Materials Chemistry A

Accepted Manuscript



This is an *Accepted Manuscript*, which has been through the Royal Society of Chemistry peer review process and has been accepted for publication.

Accepted Manuscripts are published online shortly after acceptance, before technical editing, formatting and proof reading. Using this free service, authors can make their results available to the community, in citable form, before we publish the edited article. We will replace this *Accepted Manuscript* with the edited and formatted *Advance Article* as soon as it is available.

You can find more information about *Accepted Manuscripts* in the [Information for Authors](#).

Please note that technical editing may introduce minor changes to the text and/or graphics, which may alter content. The journal's standard [Terms & Conditions](#) and the [Ethical guidelines](#) still apply. In no event shall the Royal Society of Chemistry be held responsible for any errors or omissions in this *Accepted Manuscript* or any consequences arising from the use of any information it contains.

Cite this: DOI: 10.1039/c0xx00000x

www.rsc.org/xxxxxx

ARTICLE TYPE

Inkjet-Printed Highly Conductive Transparent Patterns with Water Based Ag-Doped Graphene†

Lihong Li, Yuzhen Guo, Xingye Zhang, Yanlin Song*

Received (in XXX, XXX) Xth XXXXXXXXX 20XX, Accepted Xth XXXXXXXXX 20XX

DOI: 10.1039/b000000x

Inkjet-printing-based fabrication has been a promising approach with the rapid development and deployment of new material inks. Previous studies have demonstrated inkjet printing of reduced graphene oxide (rGO) or pristine graphene flakes produced by liquid phase exfoliation method for various devices. Nevertheless, it is still a challenge to inkjet-print conductive patterns with metal and graphene-based hybrid ink, and to explore the structure effect of metal nanoparticles on the conductivity of graphene-based transparent patterns. Herein, we present a holistic approach to achieve high-performance printed Ag nano triangle platelets-rGO (Ag NTP-rGO) and Ag polyhedral nanoparticles-rGO (Ag NPs-rGO) patterns that addresses the entire process from starting with graphene oxide exfoliation, ink formation, printing, to final reduction. Central to this approach is that the solvent of ink is only water, monodisperse Ag nano triangle platelets (Ag NTPs) and Ag polyhedral nanoparticles (Ag NPs) can be self-assembled on GO which is also used as dispersant and stabilizer, and after reduction, compared with rGO, Ag NPs-rGO and other rGO-based materials previously reported, Ag NTPs-rGO pattern displays low sheet resistance 170 Ω/\square with transmittance of 90.2%. This inkjet-printed and reduction process can be broadened to obtain other metal-graphene patterns and devices.

Introduction

Inkjet-printing-based fabrication has been a promising approach with the rapid development and deployment of new material inks.¹⁻³ This technology has advantages including digitization, additive manufacturing, reduction of material waste, and compatibility with a variety of substrates. Various technologically important active components have been inkjet-printed,⁴ including conducting electrode,⁵⁻⁶ transistors,⁷⁻⁸ solar cells,⁹ light-emitting diodes,¹⁰ battery,¹¹ and sensors.¹² However, the exploitation of patterning low-resistance electrodes with high light transmittance remains an important challenge. Although various metallic materials have been processed in solution to serve as electrodes, their inks are not stable in environmental-friendly solvents, such as water, which usually need organic addition agent,^{4, 13} and the high annealing temperature, high prices of the raw materials and the low conductivity of the electrodes limit their further applications.¹⁴⁻¹⁷

Graphene is a prominent contender as a metallic component in transparent electronic devices due to its high conductivity, chemical stability, and high transparency.¹⁸⁻²² Various approaches are applied to the production of graphene. These encompass growth by chemical vapor deposition (CVD),²³⁻²⁵ sublimation of Si atoms via heat treatment of silicon carbide,²⁶ and liquid phase exfoliation (LPE).^{6, 27} Among them, LPE offers significant advantages such as inexpensive raw materials, the potential for scalability, low thermal budget, which is ideally suited to produce

printable inks. Previous studies have demonstrated inkjet printing of reduced graphene oxide (rGO) or pristine graphene flakes produced by LPE method for organic thin-film transistor electrodes,¹⁷ temperature sensors,²⁸ radio frequency applications,²⁹ chemical sensors,¹² and electronics. Nevertheless, because the size of graphene needs to be limited in a safe range $<1/20$ of that of the small nozzle, the electrical properties of inkjet-printed LPE-synthesized graphene are unsatisfying (sheet resistance, ~ 30 $k\Omega/\square$).⁶ Recently, some researchers combined CVD-formed graphene with metal materials, such as Ag or Au nanoparticles, to improve the conductivity.³⁰⁻³¹ Moreover, a conductive rGO/Ag hybrid electrode can be formed by depositing Ag on GO nanosheets and then reducing the GO.³² However, due to the weak bonding between Ag and graphene,³³ it is difficult to obtain homogeneous Ag-graphene hybrid ink, and the mechanism of the effect of the metal structure on the improved conductivity of metal-graphene is unclear. Therefore, it is still a challenge to inkjet-print conductive patterns with metal and graphene-based hybrid ink, and to explore the structure effect of metal nanoparticles on the conductivity of graphene-based transparent patterns.

Graphene oxide (GO) nanosheet contains active groups that allow a variety of inorganic nanomaterials to be deposited on its surface.³² Herein, we present a holistic approach to achieve high-performance printed Ag nano triangle platelets-rGO (Ag NTP-rGO) and Ag polyhedral nanoparticles-rGO (Ag NPs-rGO) patterns that addresses the entire process from starting with graphene oxide exfoliation, ink formation, printing, to final

reduction. Central to this approach is that the solvent of ink is only water, and monodisperse Ag nano triangle platelets (Ag NTPs) and Ag polyhedral nanoparticles (Ag NPs) can be self-assembled on GO which is also used as dispersant and stabilizer, and after reduction, compared with rGO, Ag NPs-rGO and other rGO-based materials previously reported, Ag NTPs-rGO pattern displays low sheet resistance 170 Ω/\square with transmittance of 90.2%.

Experiment section

Materials

Graphite powder (99.998%, 200 mesh), silver nitrate (AgNO_3), L-ascorbic acid (AC), trisodium citrate dihydrate (TCD), were purchased from Alfa Aesar. Sulfuric acid (> 98%), potassium permanganate, hydrogen peroxide (H_2O_2 , 30 wt%) and sodium borohydride (NaBH_4) were purchased from Beijing Chemical Reagents, P.R. China. All chemicals were used as received without further purification.

Material preparation

Synthesis of graphene oxide (GO) sheets

GO nanosheet was synthesized according to the reported method.³⁴ The graphite powder (3 g) was added into concentrated H_2SO_4 (120 mL). Then KMnO_4 (15 g) was added gradually while stirring, and the temperature of the mixture was kept below 20 °C for 2 h using an ice bath. Successively, the mixture was stirred at 38 °C for 2 h and diluted with deionized water (500 mL) to keep the temperature at 50 °C. Additional water (420 mL) and 30% H_2O_2 (20 mL) were added, producing a brilliant yellow mixture. The mixture was filtered and washed with a 10% HCl aqueous solution to remove metal ions, which was followed by a deionized water wash to remove the acid. Then as-prepared GO was treated by ultrasonic homogenizer (4710 series, Cole Parmer Instrument Co.) under 200 W for 2 h and was passed through a 0.8 μm filter to remove large size of GO. The solid obtained on the filter was vacuum dried overnight at room temperature.

Synthesis of Ag nanoplates (Ag NTPs)

Triangular Ag nanoplates with controlled size and thickness were synthesized by a modified chemical reduction method reported by Mirkin et al.³⁵ and a seeded deposition method developed by Yin and Xia et al.³⁶⁻³⁷. A typical synthesis was described in electronic supporting information (ESI[†]). To control the size of Ag NTPs, it is needed to carefully regulate reaction time, reactant concentration, and the rate of the reactant addition.

Synthesis of Ag nanoparticles (Ag NPs)

The monodisperse Ag nanoparticles were synthesized in water according to reference.³⁸ A typical synthesis was also described in electronic supporting information (ESI[†]). Specially, the addition KI was added at low temperature (< 80 °C) to get Ag polyhedral nanoparticles (about 70 nm).

Ink Preparation

Preparation of inks for printing (Ink of GO, Ag nanoplates-GO (Ag NTPs-GO) and Ag nanoparticles-GO (Ag NPs-GO)). To form the ink of GO, the as-prepared GO was dispersed in deionized (DI) water at a concentration of 2.4 wt% by bath sonication. The resulting ink was passed through a 0.8 μm filter to remove any dust or contaminants that could destabilize printing. To form the

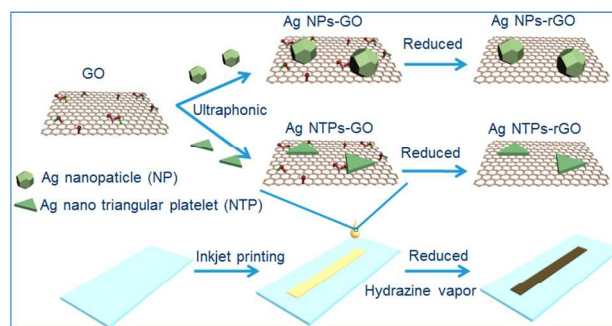


Fig. 1 Schematic illustration of the inkjet-printed patterns preparation processes.

ink of Ag NTPs-GO (or Ag NPs-GO), the Ag NTPs (or Ag NPs) were assembled on GO surface as follows: 3 mg of the Ag NTPs (or Ag NPs) dispersed in 20 mL of water was added into 20 mL of GO aqueous solution ink (1.5 mg/mL), and the mixture was treated by ultrasonic for 1 h. Then, the as-prepared Ag NTPs-GO (or Ag NPs-GO) ink was treated by the same process as GO ink, which dispersed in deionized (DI) water at a concentration of 2.4 wt% by bath sonication and then passed through the filter. The viscosity of the inks was 13.0 mPa·s for GO, 13.7 mPa·s for Ag NTPs-GO and 13.9 mPa·s for Ag NPs-GO. The surface tension of the inks was 52.3 mN/m for GO, 50.2 mN/m for Ag NTPs-GO and 49.4 mPa·s for Ag NPs-GO.

Printing

The prepared ink was injected into a cartridge for use and printed by using a Dimatix Materials Printer (FUJIFILMDMP-2800 series, Japan) with a 10 μL drop cartridge (DMC-11610). The printing was carried out at 30 °C. The glass wafers were used as substrate, which was cleaned by bath sonication in water for 20 minutes followed by drying under a stream of N_2 . The resulting water contact angle was $\sim 14^\circ$ for GO, $\sim 12.2^\circ$ for Ag NTPs-GO and 10.1° for Ag NPs-GO.

Reduction

The inkjet-printed samples were placed into a vacuum drying oven, and 1 mL of aqueous hydrazine monohydrate in a small beaker was added. They were vacuumized to about 10 Pa by a mechanical pump and then heated at 110 °C for 3 h.

Characterization

The viscosity of the inks was measured by viscometer (SV-10, A&D Company Limited, Japan) at 30 °C, and surface tension of the inks was characterized by full automatic surface tension meter (K100SF, KRÜSS GmbH Germany). The transmission electron microscopy (TEM) images were taken with a JEOL JEM-1011 transmission electron microscope operating at 100 kV. The size and structure of silver nanoparticles were characterized by a JEOL JEM-2100F transmission electron microscope operated at 200 kV, and the samples were prepared by dropping the solution onto a carbon-coated copper grid. The scanning electron microscopy (SEM) images were taken with a S-4800 (Japan Hitachi) transmission electron microscope. The transparency spectra were measured with a UV visible spectrophotometer (UV-2600, Japan Shimadzu). The structures of patterns were

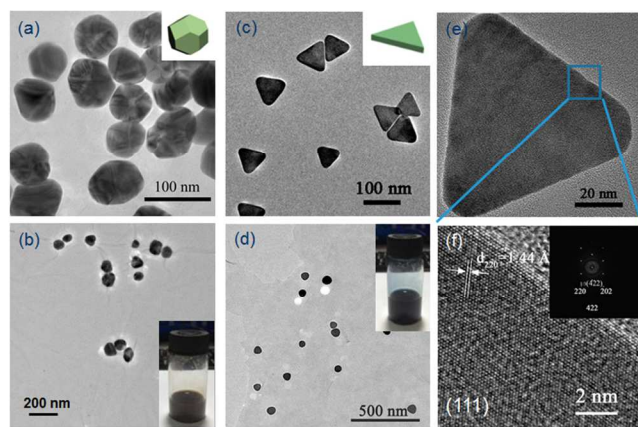


Fig. 2 The TEM images of as-synthesized (a) Ag NPs, (b) Ag NPs-GO (the inset is the photograph of the Ag NPs-GO ink), (c) Ag NTPs, (d) Ag NTPs-GO (the inset is the photograph of the Ag NTPs-GO ink) and the HRTEM image of as-synthesized (e and f) Ag NTPs, and the insert is a high resolution fast Fourier transform diffraction pattern for Ag NTPs.

investigated by an optical microscope with high speed CCD (MX40, Japan Olympus). X-ray photoelectron spectroscopy (XPS) was performed on the Thermo Scientific ESCALab 250Xi using 200 W monochromated Al K α radiation. The 500 μ m X-ray spot was used for XPS analysis. The sheet resistance and the current-voltage curve of the resulting patterns were measured by a 4-point probe nanovoltmeter (model: AS-3505C, Kasaha Laboratory Ltd., Japan).

Results and discussion

The formation process of RGO/Ag hybrid is illustrated in Fig. 1. To prepare RGO/Ag hybrid, GO suspension was firstly mixed with as-synthesized polyhedral or platelet-like Ag nanoparticles (the details of synthesis of Ag are described in the ESI \dagger), respectively, the GO-based ink was then inkjet-printed, and finally the inkjet-printed patterns were reduced in hydrazine vapor at 110 $^{\circ}$ C for further characterization and measurements.

As evidence of the different Ag particles by the TEM and SEM images shown in Fig. 2a, 2c, and S1 \dagger (see ESI), the as-obtained Ag nanoparticles (Ag NPs) are monodisperse polyhedral nanoparticles with 70 nm in diameter and Ag nano triangle platelets (Ag NTPs) with the length of perpendicular bisector also about 70 nm. To understand the structures of the composite, HRTEM analysis of Ag NTPs is performed (Fig. 2e-f). The flat exposed crystal facets are {111}, corresponding to the lattice spacing of 1.44 \AA , indexed as {220} of face-centered cubic (fcc) Ag (JCPDS card number: 04-0783). Due to citrate selectively binding to Ag (111), it favors to form Ag enclosed preferentially by {111} facets. From the high resolution fast Fourier transform diffraction pattern of Ag NTPs, it is found that the six bright spots with 6-fold symmetry can be indexed to the {220} reflections of the fcc crystal oriented in the [111] direction, and the appearance of strong diffraction spots of 1/3{422} reflections are normally forbidden for fcc Ag lattices, indicating the existence of multiple {111} twin planes parallel to the basal surfaces of the nanoplates.³⁹⁻⁴¹ The TEM images of as-prepared Ag NPs-GO and Ag NTPs-GO are shown in Fig. 2b, 2d, and S1, and the homogeneous ink of them (the insert in Fig. 2b, 2d) are

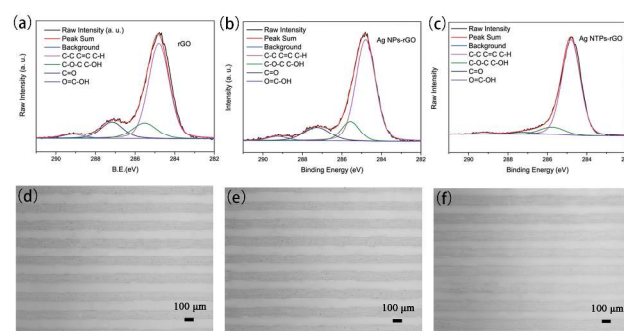


Fig. 3 The XPS spectra of C1s peaks of as-synthesized (a) rGO, (b) Ag NPs-rGO, and (c) Ag NTPs-rGO. Morphology of the inkjet-printed rGO-based patterns on glass substrates. Optical microscopy images of the printed lines of (d) rGO (e) Ag NPs-rGO and (f) Ag NTPs-rGO illustrate the uniformity of the printed features.

obtained by simply adding them in water, in which GO can be used as dispersant and stabilizer. It was found that mixing the Ag NPs or Ag NTPs with GO sheets under sonication in water led to direct self-assembly of a layer of Ag on GO, which was similar with that observed by Sun,⁴² and the Ag NTPs lay flat on the GO and the edge of Ag nanoplatelet became round.

The inkjet printing was carried out at 30 $^{\circ}$ C using a Fujifilm Dimatix Materials Printer (DMP 2800) with a cartridge designed for a 10 pL nominal drop volume. Drop spacing for all printed features was maintained at 33 μ m. The inkjet-printed samples were then reduced. To analysis the structure of the rGO-based samples, the XRD measurements were carried out (ESI, Fig. S2 \dagger). It is shown that, after reduction, the inter planar distance of the rGO is decreased to 3.69 \AA (24.6 $^{\circ}$) from 8.60 \AA (10.3 $^{\circ}$) for the original GO, due to the decrease of the oxygen-containing groups on the graphene (G) sheets. Exactly as shown in ESI, Fig. S2c \dagger , the peaks of Ag NPs-rGO at 38.1 $^{\circ}$ and 44.3 $^{\circ}$ are characteristic of face-centered cubic crystalline Ag, corresponding to the planes (111) and (200) (JCPDS card number: 04-0783). It is interesting to find that only a peak at around 38.1 $^{\circ}$ can be observed from the XRD pattern of Ag NPs-rGO, which can be assigned to the {111} plane reflection of Ag (JCPDS card number: 04-0783), and the peak at around 44.3 $^{\circ}$ almost can't be found (see ESI, Fig. S2d \dagger). It indicates that the surface planes of the product are aligned unidirectionally, normal to the {111} face on the rGO sheets. It is in agreement with the results of TEM and HRTEM (Fig. 2d, 2f), from which the Ag NTPs lying flat on the GO sheets with {111} face can be observed.

To further elucidate the reduction process, high resolution C1s peaks in the X-ray photoelectron spectroscopy (XPS) of the GO, rGO, Ag NPs-rGO, and Ag NTPs-rGO are carried out (Fig. S3 \dagger (ESI) and Fig. 3a-c). The deconvolution of the bands shows the peaks at the binding energies of 284.8 eV are attributed to the C-C, C=C, and C-H bonds, and the peaks centered at the binding energies of 285.5~285.8 eV, 287.2~287.3 eV, and 288.9~289.2 eV are assigned to the C-OH, C=O, and O=C-OH oxygen-containing carbonaceous bands, respectively, as described previously.⁴³ The detailed analysis of the C1s peak positions and the relative percentages of different C species are list in ESI, Table S1 \dagger . The percentage of C-C, C=C, and C-H bones in the

order of Ag NTPs-rGO > Ag NPs-rGO > rGO > GO, indicating that the reduction degree of rGO species is in the order of Ag

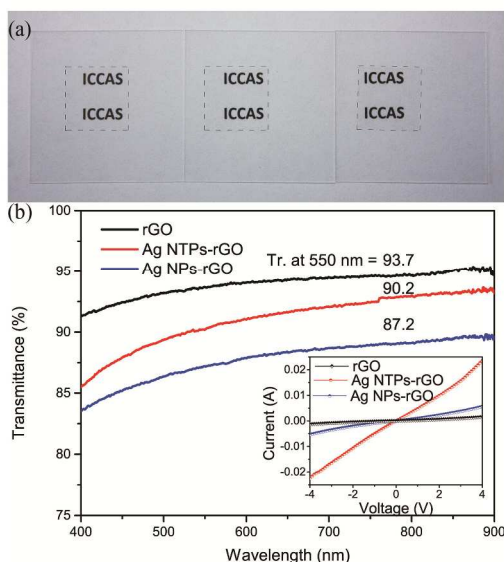


Fig. 4 (a) The transparent rGO (left), Ag NTPs-rGO (middle), and Ag NPs-rGO (right) patterns ($1 \times 1 \text{ cm}^2$) inkjet-printed on glass substrates. Analysis and comparison of transparent patterns: (b) Transparency spectra of one inkjet-printed layer of rGO, Ag NPs-rGO, and Ag NTPs-rGO inkjet-printed patterns on glass substrates. The inset shows the voltage-current IV curve of rGO, Ag NPs-rGO, and Ag NTPs-rGO range from -4 V to 4 V. The transparency (Tr.) was defined as the transmittance at a wavelength of 550 nm.

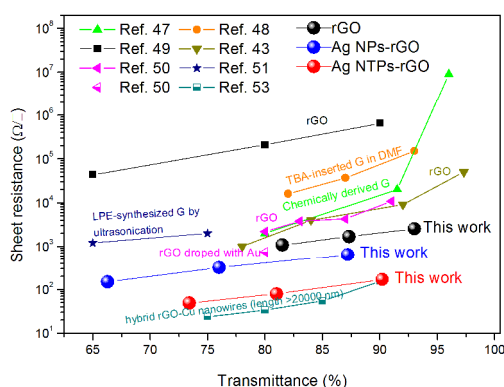


Fig. 5 Sheet resistance vs transmittance of inkjet-printed rGO-based electrodes which is corresponding to one inkjet-printed layer, two inkjet-printed layers and three inkjet-printed layers with a downward trend of the transmittance, compared to other transparent LPE-synthesized G-based electrodes from previous research results.

NTPs-rGO > Ag NPs-rGO > rGO.

From the Optical microscopy images, the patterns show no undesirable coffee ring effects, and the width of the inkjet-printed rGO-based lines on glass is about $100 \mu\text{m}$ (Fig. 3d-f, and S4† (ESI)). The fine morphology of the inkjet-printed patterns is due to the suppression of the coffee ring effect via a Marangoni flow established by the surface tension gradient.^{4, 44-45} This flow homogenizes the droplet composition, resulting in a uniform

morphology of the printed features. Furthermore, the sp² bonding, oxygen functional groups and small lateral size of the

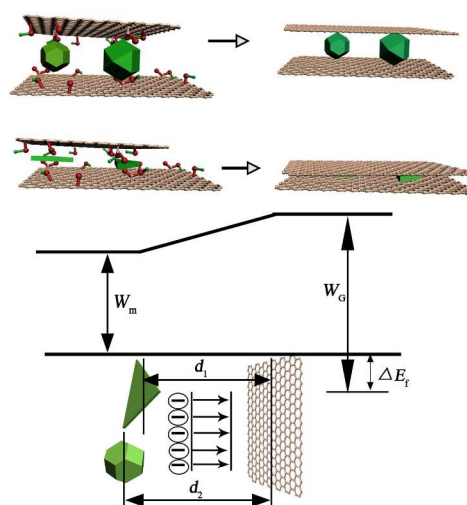


Fig. 6 Illustration of energy diagram and transportation of electrons at the graphene-metal interface.

GO flakes minimize folding or buckling of the inkjet-printed flakes, which promotes low surface roughness and well defined flake-flake contacts.

Fig. 4 shows the optical properties of inkjet-printed rGO-based patterns ($1 \times 1 \text{ cm}^2$) on glass. The transmittance data as a function of wavelength for the corresponding rGO-based inkjet-printed patterns are shown in Fig. 4b with the insert of the voltage-current (IV) curve of them range from -4 V to 4 V. Amount them, the transparency at same wavelength are in the order of: rGO > Ag NTPs-rGO > Ag NPs-rGO with the transmittance (93%, 90% and 87%) at a wavelength of 550 nm, respectively, which is enough for most transparent conducting electrode-based applications.⁴⁶ Though the addition of Ag NTPs and Ag NPs reduces the optical transmittance of Ag NTPs-rGO and Ag NPs-rGO, the transparency of Ag NTPs-rGO is higher than that of Ag NPs-rGO due to the thin thickness of Ag NTPs.

To study the electrical properties of as-prepared rGO-based patterns, different inkjet-printed layers of patterns were obtained. It is found that the sheet resistivity (R_s) of them reaches a relatively low value. Fig. 5, S5† and S6† (ESI) show sheet resistances and optical transmittances of the inkjet-printed rGO-based patterns compared to other transparent graphene-based (including LPE-synthesized G and CVD-growth G) films from previous research results. The as-prepared rGO, Ag NTPs-rGO and Ag NPs-rGO patterns have $R_s = 2.5 \text{ k}\Omega/\square$ ($T_{550} = 93\%$), $R_s = 170 \text{ }\Omega/\square$ ($T_{550} = 90\%$) and $R_s = 639 \text{ }\Omega/\square$ ($T_{550} = 87\%$), respectively, and the value of sheet resistance of rGO species is in the order of Ag NTPs-rGO < Ag NPs-rGO < rGO, which is in agreement with the reduction degree of rGO species indicated in the XPS measurement (Fig. 3). This confirms that the R_s of the rGO-based patterns are affected by the oxygen functional groups. It is found that the obtained Ag NTPs-rGO pattern with good transparency (90%) shows the lowest sheet resistance ($R_s = 170 \text{ }\Omega/\square$) amount that of LPE-synthesized G films with the similar transparent reported in references (Fig. 5).^{43, 47-51} The R_s of Ag

NTPs-rGO pattern is also lower than that of Au-doped rGO and CVD-growth G (Fig. S5† (ESI)),^{20,52} reaches the value of that of

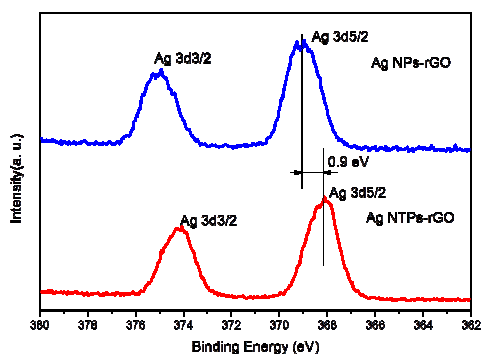


Fig. 7 The XPS patterns of Ag peaks of as-synthesized Ag NPs-rGO and Ag NTPs-rGO.

hybrid rGO-Cu nanowires (length > 20 μm , too long to be suitable for inkjet printing),⁵³ and is close to that of hydrazine-doped CVD-growth G⁵⁴ and CVD-growth G/Ag nanowires (Fig. S5† (ESI)).^{30,55}

The reasons of conductive enhancement of Ag-rGO can be explained as follows: when the GO and Ag nanoparticles (Ag NTPs, Ag NPs) is mixed, the oxygen-containing functional groups of GO contact with the silver nanoparticles. Then when the GO is reduced, the oxygen-containing functional groups are removed, the distance between silver and rGO decreases (see Fig. 6), the d orbitals of Ag interact with the π orbitals of rGO, and the conductivity of Ag nanoparticles-rGO is improved. Similar phenomenon is observed from Cu nanowire-rGO hybrid in previous report.⁵³ Especially, Ag nanoplates further enhance the conductivity of Ag NTPs-rGO. On one hand, rGO-Ag-rGO forms sandwich structure, more contacting-area between Ag and rGO is formed in Ag NTPs-rGO than Ag NPs-rGO (see Fig. 6 and S7† (ESI)), {111} plane of Ag nanoplatelet is the low energy face, and the theory distance (0.33 nm) between Ag {111} plane and graphene {001} plane is smaller than that between polyhedral Ag and graphene {001} plane,³³ which can make the electron transport between Ag and graphene easily, resulting in enhanced conductivity of Ag NTPs-rGO composite. On the other hand, the binding of Ag to rGO is important for the conductivity of the rGO-based patterns. Ag 3d XPS spectra are used to analyze the binding between Ag and reduced graphene oxide of the Ag NTPs-rGO and Ag NPs-rGO, as shown in Fig. 7. Since the work function of Ag (4.2 eV) is smaller than that of graphene (4.8 eV),⁵⁶ electron transfer from the Ag to graphene sheets can occur during the formation of the Ag-rGO heterostructures. The Ag 3d peaks shift nearly 0.9 eV to lower binding energies at 368.2 eV and 374.3 eV for Ag NTPs-rGO compared with 369.1 eV and 375.2 eV for Ag NPs-rGO, due to more electron transfer from Ag NTPs than that from Ag NPs to the rGO sheet, and the smaller distance between Ag NTPs and the rGO sheet than that between Ag NPs and the rGO sheet. Thus the conductivity of Ag NTPs-rGO is highly improved.

Conclusions

A holistic approach for achieving highly conductive inkjet-printed Ag NTP-rGO hybrid transparent patterns is demonstrated. Monodisperse Ag NTPs can be self-assembled on GO, and the low-energy {111} facet of Ag NTPs is orientational on GO {001} facets. In this system, GO is also used as dispersant and stabilizer, and water is used as solvent to prepare ink for inkjet printing. After reduction, the printed Ag NTPs-rGO pattern shows low sheet resistance $170 \Omega/\square$ with high transmittance of 90.2%. This inkjet-printed and reduction process can be broadened to obtain other metal-graphene patterns, and will be of significance for the development of metal-graphene based functional devices.

Acknowledgements

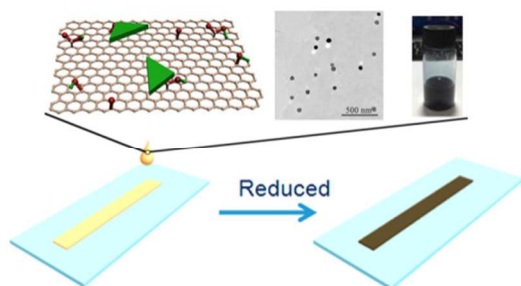
Gratefully acknowledge financial support from the National Key Scientific Program (grant numbers 2013CB933004), the NSFC (grant numbers 21301180, 51173190, 21121001, and 51473172), the ‘‘Strategic Priority Research Program’’ of the Chinese Academy of Sciences (grant number XDA09020000), and the National High Technology Research and Development Program of China (Grant No 2013AA030802).

Notes and references

- Key Laboratory of Green Printing, Institute of Chemistry, Chinese Academy of Sciences, Beijing, China. Fax: 86 6252 9284; Tel: 86 6252 9284; E-mail: ylsong@iccas.ac.cn
- † Electronic Supplementary Information (ESI) available: Synthesis of Ag nano triangle platelets and Ag polyhedral nanoparticles; The morphology and structure characterization of the as-synthesized samples via SEM, TEM, XRD and XPS; Morphology of the inkjet-printed rGO-based patterns on glass substrates; and the analysis of C1s peak positions and the relative percentages of different C species with respect to GO, rGO, Ag NPs-rGO, Ag NTPs-rGO. See DOI: 10.1039/b000000x/
- B. Y. Ahn, E. B. Duoss, M. J. Motala, X. Guo, S.-I. Park, Y. Xiong, J. Yoon, R. G. Nuzzo, J. A. Rogers and J. A. Lewis, *Science*, 2009, **323**, 1590-1593.
 - M. Kuang, L. Wang and Y. Song, *Advanced Materials*, 2014, DOI: 10.1002/adma.201305416.
 - Z. Zhang, X. Zhang, Z. Xin, M. Deng, Y. Wen and Y. Song, *Advanced Materials*, 2013, **25**, 6714-6718.
 - M. Singh, H. M. Haverinen, P. Dhagat and G. E. Jabbour, *Adv. Mater.*, 2010, **22**, 673-685.
 - E. B. Secor, P. L. Prabhurashi, K. Puntambekar, M. L. Geier and M. C. Hersam, *J. Phys. Chem. Lett.*, 2013, **4**, 1347-1351.
 - F. Torrisi, T. Hasan, W. Wu, Z. Sun, A. Lombardo, T. S. Kulmala, G.-W. Hsieh, S. Jung, F. Bonaccorso, P. J. Paul, D. Chu and A. C. Ferrari, *ACS Nano*, 2012, **6**, 2992-3006.
 - H. Yan, Z. Chen, Y. Zheng, C. Newman, J. R. Quinn, F. Dotz, M. Kastler and A. Facchetti, *Nature*, 2009, **457**, 679-686.
 - J. W. Hennek, Y. Xia, K. Everaerts, M. C. Hersam, A. Facchetti and T. J. Marks, *ACS Appl. Mater. Interfaces*, 2012, **4**, 1614-1619.
 - E. Martinez-Ferrero, I. Burgues-Ceballos, M. Stella and P. Lacharmoise, *J. Mater. Chem. A*, 2014.
 - V. Wood, M. J. Panzer, J. Chen, M. S. Bradley, J. E. Halpert, M. G. Bawendi and V. Bulović, *Adv. Mater.*, 2009, **21**, 2151-2155.
 - K. Sun, T.-S. Wei, B. Y. Ahn, J. Y. Seo, S. J. Dillon and J. A. Lewis, *Adv. Mater.*, 2013, **25**, 4539-4543.
 - V. Dua, S. P. Surwade, S. Ammu, S. R. Agnihotra, S. Jain, K. E. Roberts, S. Park, R. S. Ruoff and S. K. Manohar, *Angew. Chem. Int. Edit.*, 2010, **49**, 2154-2157.
 - N. A. Luechinger, E. K. Athanassiou and W. J. Stark, *Nanotechnology*, 2008, **19**, 445201.
 - H. Sirringhaus, T. Kawase, R. H. Friend, T. Shimoda, M. Inbasekaran, W. Wu and E. P. Woo, *Science*, 2000, **290**, 2123-2126.

15. Y. Zhao, C.-a. Di, X. Gao, Y. Hu, Y. Guo, L. Zhang, Y. Liu, J. Wang, W. Hu and D. Zhu, *Adv. Mater.*, 2011, **23**, 2448-2453.
16. L. Zhang, H. Liu, Y. Zhao, X. Sun, Y. Wen, Y. Guo, X. Gao, C.-a. Di, G. Yu and Y. Liu, *Adv. Mater.*, 2012, **24**, 436-440.
- 5 17. S. Lim, B. Kang, D. Kwak, W. H. Lee, J. A. Lim and K. Cho, *J. Phys. Chem. C*, 2012, **116**, 7520-7525.
18. R. R. Nair, P. Blake, A. N. Grigorenko, K. S. Novoselov, T. J. Booth, T. Stauber, N. M. R. Peres and A. K. Geim, *Science*, 2008, **320**, 1308.
- 10 19. W. Yuan and G. Shi, *J. Mater. Chem. A*, 2013, **1**, 10078-10091.
20. K. S. Kim, Y. Zhao, H. Jang, S. Y. Lee, J. M. Kim, K. S. Kim, J.-H. Ahn, P. Kim, J.-Y. Choi and B. H. Hong, *Nature*, 2009, **457**, 706-710.
21. J. U. Park, S. Nam, M. S. Lee and C. M. Lieber, *Nat. Mater.*, 2012, 15 **11**, 120-125.
22. S. J. Guo, S. Zhang and S. H. Sun, *Angew Chem Int Edit*, 2013, **52**, 8526-8544.
23. X. Li, W. Cai, J. An, S. Kim, J. Nah, D. Yang, R. Piner, A. Velamakanni, I. Jung, E. Tutuc, S. K. Banerjee, L. Colombo and R. S. Ruoff, *Science*, 2009, **324**, 1312-1314.
- 20 24. K. S. Novoselov, V. I. Falko, L. Colombo, P. R. Gellert, M. G. Schwab and K. Kim, *Nature*, 2012, **490**, 192-200.
25. W. J. Fang, A. L. Hsu, Y. Song, A. G. Birdwell, M. Amani, M. Dubey, M. S. Dresselhaus, T. Palacios and J. Kong, *ACS Nano*, 2014, **8**, 6491-6499.
26. Y.-M. Lin, C. Dimitrakopoulos, K. A. Jenkins, D. B. Farmer, H.-Y. Chiu, A. Grill and P. Avouris, *Science*, 2010, **327**, 662.
27. W. S. Hummers and R. E. Offeman, *J. Am. Chem. Soc.*, 1958, **80**, 1339-1339.
- 30 28. D. Kong, L. T. Le, Y. Li, J. L. Zunino and W. Lee, *Langmuir*, 2012, **28**, 13467-13472.
29. K.-Y. Shin, J.-Y. Hong and J. Jang, *Adv. Mater.*, 2011, **23**, 2113-2118.
30. I. N. Kholmanov, C. W. Magnuson, A. E. Aliev, H. Li, B. Zhang, J. W. Suk, L. L. Zhang, E. Peng, S. H. Mousavi, A. B. Khanikaev, R. Piner, G. Shvets and R. S. Ruoff, *Nano Lett.*, 2012, **12**, 5679-5683.
- 35 31. K. K. Kim, A. Reina, Y. Shi, H. Park, L.-J. Li, Y. H. Lee and J. Kong, *Nanotechnology*, 2010, **21**, 285205.
32. L. Lu, J. Liu, Y. Hu, Y. Zhang and W. Chen, *Adv. Mater.*, 2013, **25**, 40 1270-1274.
33. G. Giovannetti, P. A. Khomyakov, G. Brocks, V. M. Karpan, J. van den Brink and P. J. Kelly, *Phys. Rev. Lett.*, 2008, **101**, 026803.
34. L. H. Li, Y. e. Wu, J. Lu, C. Y. Nan and Y. D. Li, *Chem. Commun.*, 2013, **49**, 7486-7488.
- 45 35. G. S. Métraux and C. A. Mirkin, *Adv. Mater.*, 2005, **17**, 412-415.
36. Q. Zhang, Y. Hu, S. Guo, J. Goebel and Y. Yin, *Nano Lett.*, 2010, **10**, 5037-5042.
37. J. Zeng, X. Xia, M. Rycenga, P. Henneghan, Q. Li and Y. Xia, *Angew. Chem. Int. Edit.*, 2011, **50**, 244-249.
- 50 38. H. Li, H. Xia, D. Wang and X. Tao, *Langmuir*, 2013, **29**, 5074-5079.
39. R. Jin, Y. Charles Cao, E. Hao, G. S. Métraux, G. C. Schatz and C. A. Mirkin, *Nature*, 2003, **425**, 487-490.
40. D. Aherne, D. M. Ledwith, M. Gara and J. M. Kelly, *Adv. Funct. Mater.*, 2008, **18**, 2005-2016.
- 55 41. Q. Zhang, N. Li, J. Goebel, Z. Lu and Y. Yin, *J. Am. Chem. Soc.*, 2011, **133**, 18931-18939.
42. S. Guo and S. Sun, *J. Am. Chem. Soc.*, 2012, **134**, 2492-2495.
43. H. A. Becerril, J. Mao, Z. Liu, R. M. Stoltenberg, Z. Bao and Y. Chen, *ACS Nano*, 2008, **2**, 463-470.
- 60 44. H. Masoud and H. A. Stone, *J. Fluid Mech.*, 2014, **741**.
45. J. A. Lim, W. H. Lee, H. S. Lee, J. H. Lee, Y. D. Park and K. Cho, *Adv. Funct. Mater.*, 2008, **18**, 229-234.
46. Y. Zhu, Z. Sun, Z. Yan, Z. Jin and J. M. Tour, *ACS Nano*, 2011, **5**, 6472-6479.
- 65 47. H. Yamaguchi, G. Eda, C. Mattevi, H. Kim and M. Chhowalla, *ACS Nano*, 2010, **4**, 524-528.
48. X. Li, G. Zhang, X. Bai, X. Sun, X. Wang, E. Wang and H. Dai, *Nat Nano*, 2008, **3**, 538-542.
49. G. Eda, G. Fanchini and M. Chhowalla, *Nat Nano*, 2008, **3**, 270-274.
- 70 50. S. Y. Jeong, S. H. Kim, J. T. Han, H. J. Jeong, S. Yang and G.-W. Lee, *ACS Nano*, 2011, **5**, 870-878.
51. A. A. Green and M. C. Hersam, *Nano Lett.*, 2009, **9**, 4031-4036.
52. X. Li, Y. Zhu, W. Cai, M. Borysiak, B. Han, D. Chen, R. D. Piner, L. Colombo and R. S. Ruoff, *Nano Lett.*, 2009, **9**, 4359-4363.
- 75 53. I. N. Kholmanov, S. H. Domingues, H. Chou, X. Wang, C. Tan, J.-Y. Kim, H. Li, R. Piner, A. J. G. Zarbin and R. S. Ruoff, *ACS Nano*, 2013, **7**, 1811-1816.
54. J. B. Bult, R. Crisp, C. L. Perkins and J. L. Blackburn, *ACS Nano*, 2013, **7**, 7251-7261.
- 80 55. M.-S. Lee, K. Lee, S.-Y. Kim, H. Lee, J. Park, K.-H. Choi, H.-K. Kim, D.-G. Kim, D.-Y. Lee, S. Nam and J.-U. Park, *Nano Lett.*, 2013, **13**, 2814-2821.
56. T. Wu, H. Shen, L. Sun, B. Cheng, B. Liu and J. Shen, *ACS Appl. Mater. Interfaces*, 2012, **4**, 2041-2047.
- 85

Table of contents entry



Transparent Ag nano triangle platelets-rGO (Ag NTP-rGO) pattern with highly conductive was obtained by inkjet-printing of Ag NTPs-rGO ink, the solvent of which is only water.